Title: Bioengineering of the implantable vascularized endocrine constructs for insulin delivery suitable for clinical upscaling

Authors: Kevin Bellofatto[1,2†], Fanny Lebreton[1,2†], Masoud Hassany[1‡], Reine Hanna[1,2], Juliette Bignard[1,2], Antoine Marteyn[1,2], Laura Mar Fonseca[1,2], Francesco Campo[8], Cristina Olgasi[7], Lelia Wolf-van Bürck[10], Mohsen Honarpisheh[10], Begoña Martinez de Tejada[11], Antonia Follenzi[6], Antonio Citro[8], Lorenzo Piemonti[8], Olivier Thaunat[9], Jochen Seissler[10], Phillippe Compagnon[1,3], Marie Cohen[11], Ekaterine Berishvili[1,2,3,4,5*] and VANGUARD consortium[§]

Affiliations:

[1]Cell Isolation and Transplantation Centre, Department of Surgery, Geneva University Hospitals, Geneva, Switzerland

[2]Laboratory of Tissue Engineering and Organ Regeneration, Department of Surgery, University of Geneva, Geneva, Switzerland

[3]Division of Transplantation, Department of Surgery, University of Geneva Hospitals, Geneva, Switzerland

[4]Faculty Diabetes Center, University of Geneva School of Medicine, Geneva, Switzerland

[5]Institute of Medical and Public Health Research, Ilia State University, Tbilisi, Georgia

[6]Department of Health Sciences, University of Piemonte Orientale, Novara, Italy

[7]Department of Translational Medicine, University of Piemonte Orientale, Novara, Italy

[8]IRCCS Ospedale San Raffaele, Diabetes Research Institute, Milano, Italy

23 [9]Lyon Claude Bernard University, Dept. Transplantation, Nephrology and Clinical Immunology,
24 Lyon, France
25 [10]Medizinische Klinik und Poliklinik IV, Diabetes Zentrum, Klinikum der Universität München,
26 LMU Munich, Germany
27 [11]Department of Pediatrics, Gynecology and Obstetrics, Faculty of Medicine, Geneva, Switzerland
28
29 *Corresponding author. Email: Ekaterine.berishvili@unige.ch
30 †These authors contributed equally to this work
31 ‡Present address: Department of Civil and Mechanical Engineering, Technical University of
32 Denmark, 2800 Kgs. Lyngby, Denmark
33
34 **One Sentence Summary:** A clinically scalable, biological hydrogel based vascularized
35 endocrine constructs show sustained diabetes reversal.
36
37
38
39
40
41
42

Abstract:

Beta cell replacement therapy for type 1 diabetes is hindered by poor graft survival and suboptimal function, largely due to inadequate vascularization and lack of supportive microenvironment. To address these challenges, we developed a clinically scalable, extracellular matrix (ECM)–mimetic hydrogel, termed Amniogel, derived from human amniotic membrane via streamlined, clinically compliant process. Co-encapsulation of pancreatic islets with blood outgrowth endothelial cells (BOECs) within Amniogel facilitated the formation of prevascularized endocrine constructs (VECs). These constructs demonstrated enhanced β-cell viability and function through ECM-bound pro-survival signals, rapid self-assembly of perfusable endothelial networks enabling efficient glucose sensing, and deposition of laminin-rich basement membranes enhancing β-cell coupling and insulin secretion kinetics. In preclinical diabetic mouse models, VECs rapidly integrated with the host vasculature and provided sustained glycemic control when implanted subcutaneously. This integrative approach, combining a scalable, cost-effective biological scaffold with autologous vascularization potential, represents a significant advancement toward durable and clinically translatable β-cell replacement therapies for T1DM.

66 **INTRODUCTION**

67 Type 1 diabetes mellitus (T1DM) results from autoimmune destruction of insulin-producing β-
68 cells, and while insulin therapy is the standard treatment, it does not prevent long-term
69 complications or ease the daily management burdens (*1*). Intrahepatic islet transplantation
70 temporarily restores insulin independence and improves glycemic control (*2*). However, its
71 widespread clinical implementation is hindered by donor islet scarcity and the risks associated
72 with lifelong immunosuppression (*3-6*). Moreover, instant blood-mediated inflammatory reaction
73 (IBMIR), oxidative stress, loss of extracellular matrix (ECM) signals and poor vascularization
74 significantly compromise islet engraftment and function in the liver (*7-10*). Extrahepatic
75 transplantation sites are being explored to overcome these issues (*11-19*). Amongst these, the
76 subcutaneous space is gaining interest due to its safety, large surface area, and accessibility for
77 implantation and monitoring. However, inadequate vascularization and hypoxia frequently lead to
78 islet graft failure (*20, 21*).

79 Tissue-engineering approaches aim to mitigate these issues using supportive scaffolds or
80 encapsulation devices. Diverse macrodevices made of synthetic polymers have been designed to
81 house islets or stem cell–derived islet-like clusters (*22*). Although some have advanced to first-in-
82 human trials, clinical success has been limited due to fibrosis, foreign body response, and
83 inadequate vascularization (*23-25*). Critically, macro-devices designed so far rely on inorganic or
84 synthetic polymers, which fail to deliver the native ECM cues and vascularization essential for β-
85 cell survival and function.

86 Islets are abundantly vascularized miniorgans surrounded by specialized extracellular matrix
87 essential for β-cell viability and proper function (*26*). The isolation process disrupts this
88 irreversibly disrupts this dynamic microenvironment, triggering β-cell apoptosis (*27*). Integrating

ECM components with endothelial cells has been shown to improve islet survival and function in preclinical models (*28-32*). Yet, the clinical translation of these strategies remains challenging. An ideal construct would combine a biocompatible biological ECM with a built-in, high-density, functional vascular network in direct contact with encapsulated islets, enabling prompt revascularization, efficient glucose sensing and insulin secretion, and be readily scalable for clinical translation.

Here, we report a clinically scalable strategy to engineer vascularized endocrine constructs for subcutaneous implantation. We first generated Amniogel, an ECM-mimetic hydrogel derived from the human amniotic membrane, suitable for low-cost, clinical-grade manufacturing. By co-encapsulating pancreatic islets and blood outgrowth endothelial cells (BOECs) within this biologic platform, we engineered prevascularized endocrine constructs that replicate key aspects of the native islet niche through three synergistic mechanisms: 1) preservation of β-cell viability and function via essential ECM-bound pro-survival signals, 2) self-assembly of perfusable endothelial networks directly interfacing with islets to enable rapid glucose sensing and 3) deposition of laminin-rich basement membrane components that enhance β-cell gap junction coupling and insulin secretion kinetics. Importantly, engineered constructs demonstrated rapid vascular integration and sustained glycemic control in diabetic mice in two clinically relevant extrahepatic sites—the epididymal fat pad (as an omental analog in rodents) (*33, 34*) and the subcutaneous space. This synergistic strategy, integrating a clinically scalable biomaterial with autologous vascularization potential, represents a promising advance toward clinically translatable, durable cell therapies for type 1 diabetes.

112 **RESULTS**

113 **Production and characterization of Amniogel**

114 To enable clinical translation of Amniogel, we developed a five-step, Good Manufacturing
115 Practice (GMP)-compliant production protocol (Fig. 1A). Human amniotic membrane (hAM) was
116 decellularized using xenogen-free 10X TrypLE™ Select, effectively reducing DNA content from
117 424.0 ± 58.15 ng/mg in native tissue to 38.03 ± 2.24 ng/mg, below the biocompatibility threshold
118 of <50 ng/mg (Fig 1B) (*35*). Biochemical profiling showed retention of collagen, although
119 glycosaminoglycan content was partially decreased from 8.83 ± 1.18 to 3.59 ± 1.16 µg/mg (Fig.
120 1C–D).

121 Following these initial assessments, we analyzed ECM protein retention post-decellularization
122 using mass spectrometry. Across all analyzed samples—native human amniotic membrane (hAM),
123 decellularized hAM (dAM), and three independent batches of Amniogel—we identified a total of
124 499 proteins. After removing contaminants, sample preparation enzymes, and proteins with a false
125 discovery rate (FDR) below 95%, 452 proteins remained for analysis (Fig. 1E). We then filtered
126 this dataset to focus on ECM proteins known to support islet survival and function (*36*). Among
127 these six were consistently retained in all three Amniogel batches, including collagen alpha-1(I)
128 chain, collagen alpha-1(III) chain, collagen alpha-2(I) chain, collagen alpha-3(VI) chain, and
129 fibrillin-1. Notably, essential cell-binding proteins such as fibronectin were detected, although at
130 reduced abundance. All three independently produced Amniogel batches exhibited highly similar
131 ECM protein profiles, demonstrating robust batch-to-batch reproducibility (Fig.1F).

132 Amniogels were formulated with ECM concentrations of 2.5–10 mg/ml. Formulations at 5–
133 10 mg/mL exhibited enhanced structural rigidity, facilitating easy handling and manipulation with
134 forceps (Fig.1G). SEM analysis of Amniogels revealed an inverse relationship between ECM

concentration in hydrogel and pore size (0.5712 ± 0.3099 µm at 2.5 mg/mL vs 0.1845 ± 0.08926 µm at 10 mg/mL; Fig. 1H, I). The 5 mg/mL concentration was selected for subsequent experiments due to its optimal balance between handling properties and a pore size that favors the diffusion of oxygen and nutrients. TEM further confirmed that collagen fiber integrity was preserved compared to native hAM (Fig. 1J).

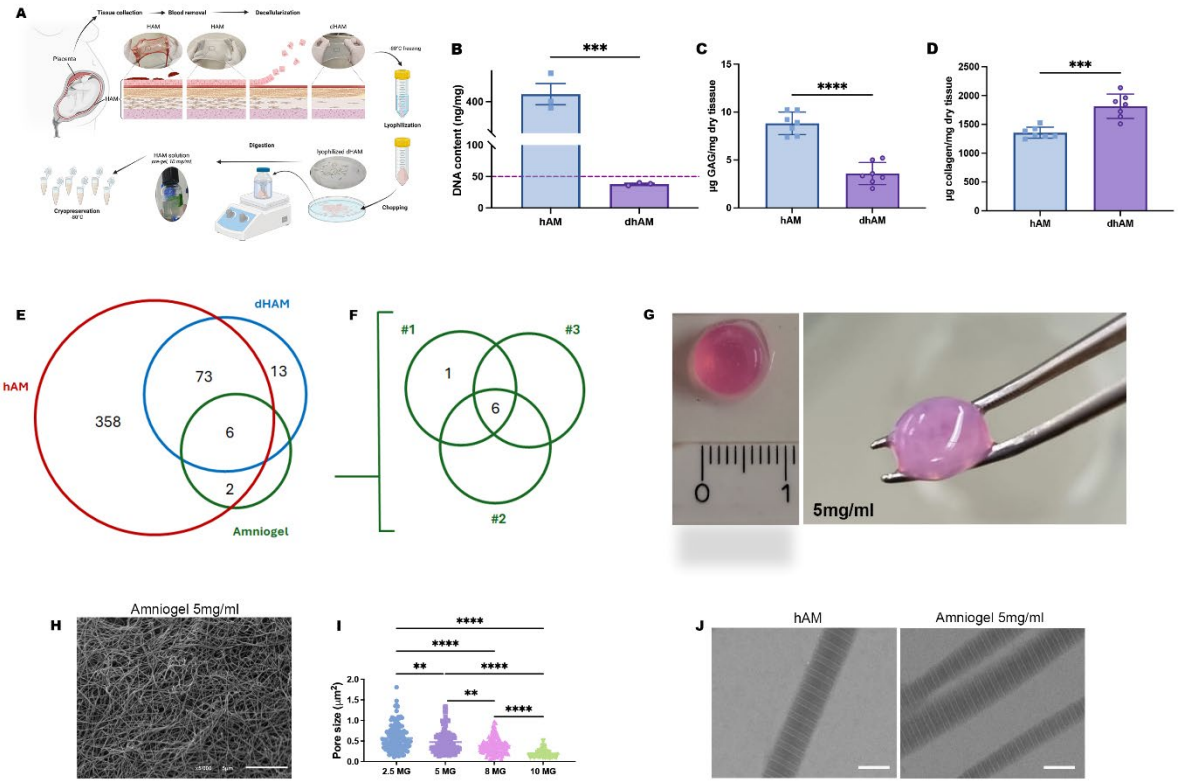

Figure 1 Generation and characterization of Amniogel (A) Schematic representation of Amniogel preparation. (B) DNA quantification in fresh (hAM) and decellularized (dHAM) human amniotic membranes. Data are presented as mean ± SD, two-tailed unpaired t-test, ***p = 0.0003 (n = 3 biological replicates). (C, D) Quantification of collagen, and GAGs. Data are presented as mean ± SD, two-tailed unpaired t-test, ****p <0.0001, ***p = 0.0002 (n = 7 biological replicates).

(E, F) Comparative analysis of ECM protein retention across fresh hAM, dHAM and Amniogel. Venn diagram highlights 92 proteins retained post-decellularization, with six proteins shared across all conditions, including Collagen alpha-1(I), Collagen alpha-2(I), Collagen alpha-3(VI), and Fibrillin-1. The reproducibility of Amniogel protein composition was confirmed across three independent batches, with six proteins consistently retained across all batches and one protein identified in individual batches. (G) Macroscopic view of Amniogel at 5 mg/ml. (H) SEM images of Amniogel (5 mg/ml) displaying an interconnected fibrous network. Scale bars, 5 µm. (I) Pore size analysis of Amniogel. A progressive reduction in pore size was observed between 2.5 and 5 mg/mL, with a pronounced decrease at 8 and 10 mg/mL. Data are presented as mean ± SD, one-way ANOVA with Tukey's correction: 2.5 mg/ml vs. 5 mg/ml, **p=0.0025; 2.5 mg/ml vs. 8 mg/ml, ****p<0.0001; 2.5 mg/ml vs. 10 mg/ml,****p <0.0001; 5 mg/ml vs. 8 mg/ml, **p=0.0097; 5 mg/ml vs. 10 mg/ml ****p<0.0001; 8 mg/ml vs. 10 mg/ml, ****p<0.0001. Depicted are the mean values of 138 detected pores from six random areas per sample (n = 3 biological replicates). (J, K) TEM analysis revealed no discernible differences in the fiber structure of collagen within Amniogel compared to native human amniotic membrane (hAM). Scale bars, 500 nm.

169 Gelation kinetics of Amniogel were comparable to those of rat tail collagen type I (Fig. S1).
170 Amniogel demonstrated robust cytocompatibility and the capacity for cell-driven remodeling.
171 Our observations show that Amniogel contraction is influenced by both the concentration of
172 decellularized hAM and the cell seeding density. Specifically, when seeded with BOECs, gels with
173 lower stiffness (5 mg/mL) contracted to 37% of their initial area, while stiffer 8 mg/mL gels
174 retained 96% of their original dimensions (Fig. S2A, B). Over seven days, BOECs in 5 mg/mL
175 gels progressively reorganized into interconnected capillary-like networks, whereas 8 mg/mL gels
176 restricted morphogenesis to fragmented, short structures (Fig. S2C). This suggests that Amniogel
177 at 5 mg/mL provides an optimal balance of stiffness, enabling matrix remodeling and supporting
178 reproducible vessel formation.
179 Furthermore, BOECs cultured on Amniogel-coated plates showed a significant increase in cell
180 numbers relative to collagen controls, adopting spindle-shaped morphologies and proliferating
181 over seven days (Fig. S3A, B). Viability (FDA/PI) assays confirmed minimal cytotoxicity, with
182 >90% cell survival across all conditions, validating Amniogel's biocompatibility (Fig. S3C).
183 These results demonstrate that Amniogel is a biocompatible scaffold that retains essential ECM
184 components crucial for islet viability and function, while supporting cell attachment and matrix
185 remodeling.
186

187 **Islet survival and function in Amniogel**

188 We next evaluated whether Amniogel encapsulation protects and improves islet function. Under
189 normoxic conditions (20% O_2), viability of rat islets embedded in Amniogel was similar to controls
190 cultured in suspension (Fig. S4A, C, E). However, suspension-cultured islets formed clumps and
191 developed necrotic cores over time. Under hypoxic conditions (1% O_2 for 16 h), suspended islets

192 showed extensive necrosis, while Amniogel-embedded islets maintained high viability (Fig. S4B
193 to E). Notably, Amniogel-embedded islets demonstrated significantly enhanced glucose-
194 stimulated insulin secretion and a higher stimulation index (SI: 0.7 ± 0.3 vs 2.3 ± 0.95, p = 0.05)
195 compared to hypoxic controls (Fig. S4F). These results suggest that Amniogel attenuates hypoxic
196 injury and preserves islet functionality under stress.
197 To evaluate the impact of cellular adhesion to Amniogel on human β-cell function and viability,
198 human islets were embedded in Amniogel to form endocrine constructs (hEC) or maintained in
199 standard suspension culture (HI alone) as controls for 7 days. Islets embedded in Amniogel
200 retained their normal morphology and hormone expression (Fig. 2A,B). Basal insulin release was
201 reduced in hECs, suggesting improved glucose regulation (Fig. S5A). Furthermore, hECs showed
202 significantly enhanced insulin secretion both under high-glucose stimulation (SI: 2.317 ± 0.195 vs
203 1.204 ± 1.135, p = 0.0012) and theophylline stimulation (SI: 4.240 ± 0.673 vs 2.385 ± 0.110, p =
204 0.0092) compared to HI alone (Fig. S5B, C). To elucidate mechanisms underlying enhanced
205 insulin secretion in hECs, we analyzed β1-integrin expression. Immunofluorescence revealed a
206 significantly increased β1-integrin expression in Amniogel-embedded islets compared to controls
207 (Fig. 2C, D). This was confirmed by qPCR, showing a threefold increase in *ITGB1* expression (p=
208 0.0016; Fig. 2E). The elevated β1-integrin expression was associated with significantly reduced
209 pro-apoptotic *CASP3* expression (p = 0.0003) and increased anti-apoptotic *BCL2* expression by a
210 4.8-fold (p=0.0089; Fig. 2F, G).
211 These findings demonstrate that Amniogel promotes β-cell viability, structural integrity, and
212 insulin secretion by enhancing cellular interactions and reducing apoptosis.
213

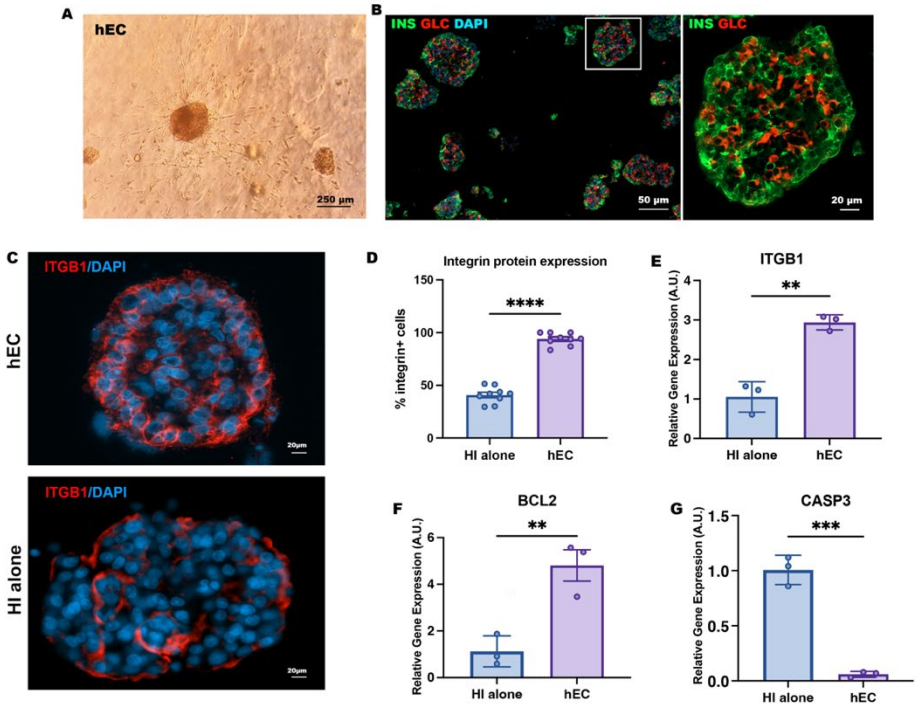

Figure 2 Amniogel Enhances Human Islet Viability and Function (A, B) Optical microscopy and immunofluorescent images of Amniogel-embedded human islets cultured for 7 days. Islets were stained for insulin (green) and glucagon (red). (C–D) Representative immunofluorescence images and quantification of β1-integrin expression in hECs and human islets in suspension. Data are presented as mean ± SD, two-tailed unpaired t-test, ****$p < 0.0001$. (E-G) qPCR of *ITGB CASP3* and *BCL2* on hECs and HI alone. Data are presented as arbitrary units (AU) after normalization to housekeeping genes, mean ± SD, two-tailed unpaired t-test, *ITGB,* **$p = 0.0016$; *BCL2*, **$p = 0.0089$; *CASP3*, ***$p = 0.0003$ (n = 3 biological replicates).

Amniogel supports endothelial cell self-organization into a vascular network

To evaluate Amniogel's ability to support endothelial cell self-organization, LV-GFP BOECs were embedded in Amniogel and cultured in vasculogenic media (VM) (Fig. 3A).

Cells formed interconnected structures within 48 hours, evolving into a robust vascular network by day 7 (Fig. 3B). Individual cells were no longer distinguishable, indicating their complete integration into continuous tubular structures (Fig. 3C). Functional validation was demonstrated by Texas red–labeled dextran perfusion into hollow lumens, confirming effective fluid transport (Fig. 3D). Immunostaining further demonstrated that the vessel-like structures were surrounded by a basement membrane, as evidenced by collagen type IV deposition (Fig. 3E). These findings indicate that Amniogel provides a supportive microenvironment facilitating endothelial cell self-organization into functional vascular networks.

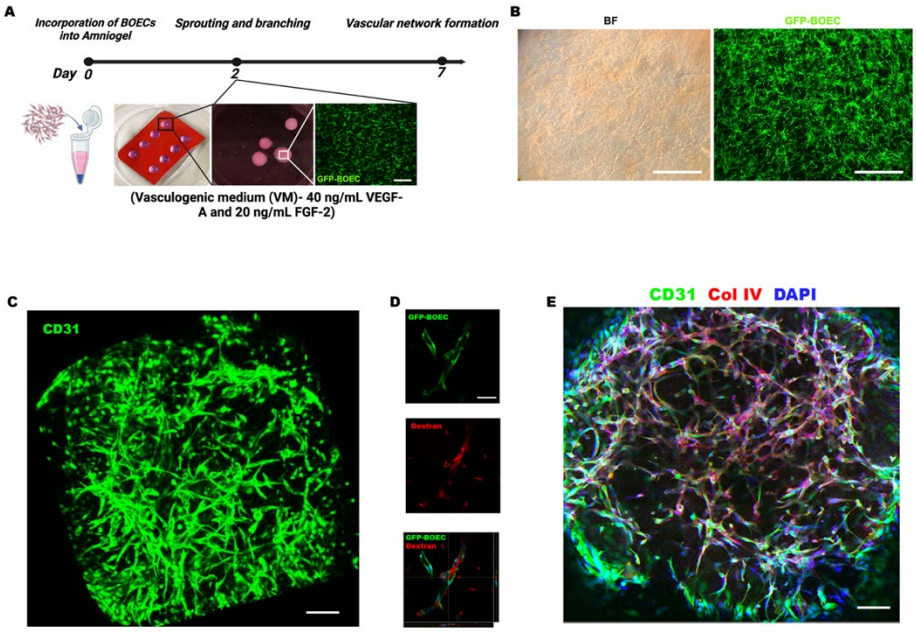

Figure 3 Amniogel Facilitates Formation of vascular networks. (A) Schematic representation of vascular construct generation. Scale bars, 500 µm. Created in https://BioRender.com (B) Representative bright-field and immunofluorescence images of LV-GFP transduced BOECs

257 showing the establishment of vascular networks. Scale bars, 500 μm. (C) 3D reconstruction of
258 capillary organization (CD31, green) in a vascular construct. Scale bars, 50 μm. (D) Formation of
259 hollow endothelial structures within 3D constructs, visualized through virtual stacks of LV-GFP
260 transduced BOECs incubated with Texas Red-labeled dextran. Scale bars, 30 μm. (E) Whole-
261 mount immunofluorescence of vascular networks showing endothelial cells (CD31, green) and the
262 vascular basement membrane (Col IV, red). Scale bars, 50 μm.

263

264

265 **Generation of vascularized endocrine constructs**

266 We hypothesized that Amniogel could facilitate the synergistic interaction between endothelial
267 cells and pancreatic islets, thereby supporting the development of more complex vascularized
268 endocrine constructs (hVECs). To test this hypothesis, we incorporated both human derived islets
269 and BOECs into Amniogel and cultured them for 7 days in optimized vasculogenic medium
270 (OVM) (Fig. 4 A). Within 3 days, BOECs formed continuous 3D vascular networks around islets
271 (Fig. 4B). Interestingly, despite the initial lack of laminin in Amniogel, the islets were surrounded
272 by a laminin-rich matrix (Fig. 4C). qPCR analysis identified BOECs as the primary laminin source,
273 showing a 3.9-fold increase in *LAMB1* expression in hVECs ($p=0.008$) and 5.7-fold in BOECs
274 ($p=0.0003$) versus HI alone (Fig. 4D). This indicates that BOECs play a critical role in laminin
275 deposition within the gel, leading to the development of a physiological-like ECM surrounding the
276 islets.

277

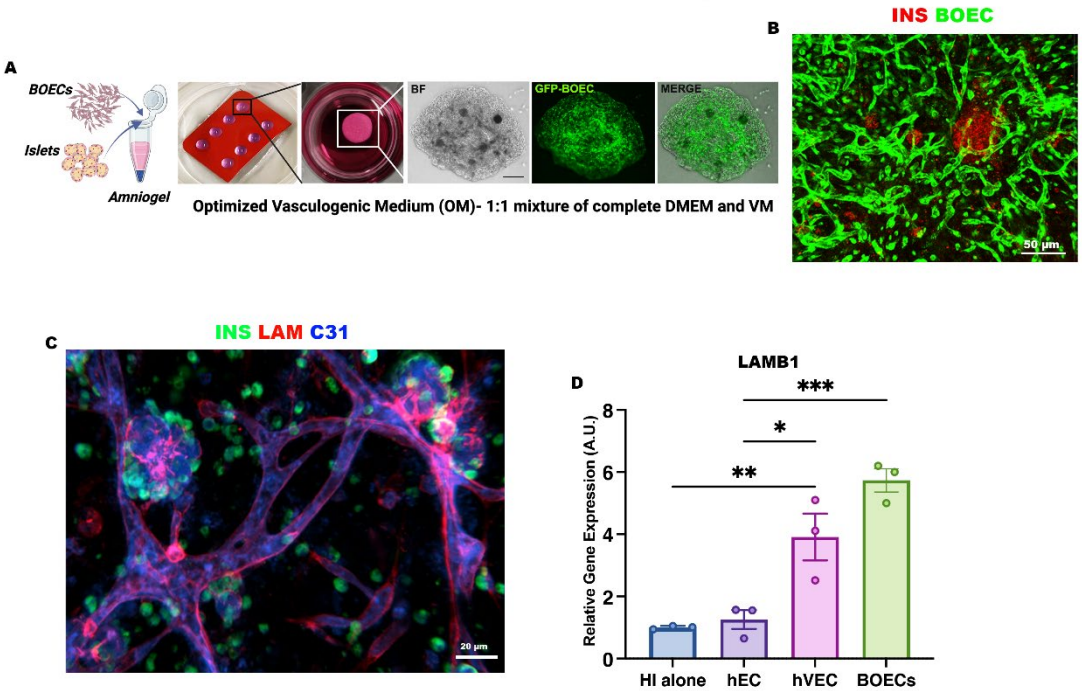

Figure 4 Assembly of hVECs. (A) Schematic representation of hVEC assembly. Representative bright-field and immunofluorescence images of hVECs demonstrate the formation of a dense vascular network (green, GFP-transduced BOECs) surrounding the embedded islets. Scale bar, 200 µm. Created in https://BioRender.com. (B) Representative confocal fluorescence microscopy images of hVEC reveal vessel formation (green, GFP-transduced BOECs) adjacent to islets (insulin, red). Scale bar, 50mm. (C) Immunofluorescent staining of laminin (red) highlights the presence of basement membrane encasing islets (insulin, green) and CD31+ endothelium (blue). Scale bar, 20mm.

To explore functional implications of vascular integration, we investigated the role of gap junctions, specialized membrane domains composed of nonspecific channels that facilitate cell-to-cell communication, which is essential for coordinated insulin release (Fig. 5A) (*37*). qPCR analysis revealed significant upregulation of *GJD2,* with increases observed in both hECs and hVECs (5.3-fold, $p = 0.0057$, and 8.8-fold, $p < 0.0001$, respectively) compared to HI alone (Fig. 5B). Similarly, expression of *GJA1* increased notably, rising 6.3-fold in hECs ($p = 0.0042$) and 11.4-fold in hVECs ($p < 0.0001$) relative to controls (Fig. 5C), indicating strong coupling between β cells and endothelial cells. Consistent with these molecular findings, functional glucose-stimulated insulin secretion (GSIS) assays showed superior performance in vascularized constructs, characterized by reduced basal secretion and increased glucose responsiveness (Fig. S6). Together, these data suggest engineered vasculature within Amniogel enhances islet function through dual mechanisms: (i) BOEC-derived laminin deposition recapitulating native peri-islet ECM, and (ii) connexin-mediated cell–cell communication essential for coordinated insulin release.

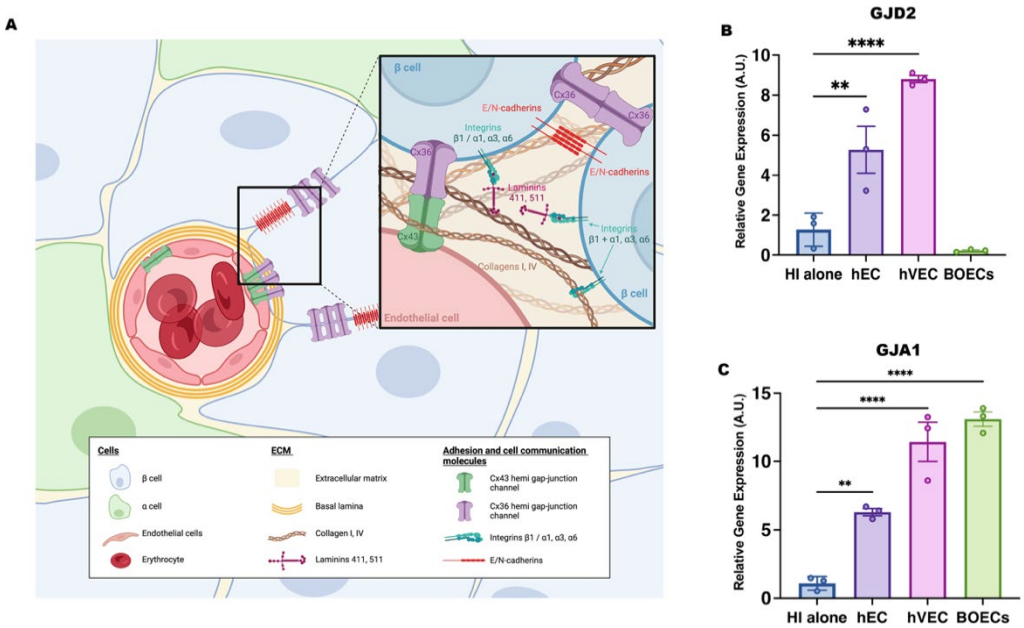

Figure 5 Engineering vasculature within amniogel promotes islet intercellular and cell-to-matrix communication. (A) Graphical illustration of known intercellular and ECM–cell interactions within islets. Cell adhesion molecules enhance β-cell glucose responsiveness, while connexin 36 and connexins 36/43 mediate insulin release by coordinating communication between β-cells and endothelial cells. Cadherins support cell–cell adhesion and inhibit apoptosis in α and β- cells. The ECM, enriched with laminin-211, laminin-511, and type IV collagen, forms a microenvironment that promotes granule secretion, cell proliferation, and apoptosis inhibition. Integrins bind ECM components like collagen and laminin, activating signaling cascades that regulate cell survival, growth, and differentiation. Created in https://BioRender.com (B, C) qPCR of *GJD2 and GJA1* in hECs, hVECs and HI alone. Data are presented as arbitrary units (AU), normalized to housekeeping genes, and shown as mean ± SD. One-way ANOVA with Tukey's correction, *GJD2:* hEC vs HI alone, **p = 0.0057; hVEC vs HI alone, ****p<0.0001; HI alone vs BOECs, n.s. p= 0.5452 (n = 3 biological replicates); *GJA1*: hEC vs HI alone, **p = 0.0042; hVEC vs HI alone, **** p<0.0001; HI alone vs BOECs, **** p<0.0001 (n = 3 biological replicates).

329 **In vivo biocompatibility**

330 To determine whether Amniogel triggers an immune response upon transplantation, empty
331 hydrogels were transplanted subcutaneously into immunocompetent C57BL/6 mice (Fig. S7A).
332 Grafts were harvested 1month post-implantation and analyzed histologically. H&E staining
333 revealed modest mononuclear cell infiltration at the implantation sites without granuloma
334 formation, indicating minimal local toxicity and high tissue compatibility (Fig. S7B). Masson's
335 trichrome staining demonstrated preserved collagen fibrils in the Amniogel. Spindle-shaped cells,
336 likely fibroblasts, were also observed within the grafts. Immunohistochemical staining for CD45
337 and CD11b confirmed that immune cell infiltration in transplanted acellular gels was comparable
338 to that in sham-operated controls (Fig. S7B).

339 **Site-specific engraftment of non-vascularized endocrine constructs**

340 We then tested the performance of the Amniogel-based constructs in vivo using streptozotocin-
341 diabetic NSG immunodeficient mice (Fig. 6A). In the highly vascularized epididymal fat pad
342 (EFP) site, even non-vascularized endocrine constructs (EFP-rEC) significantly outperformed islet
343 transplanted alone (EFP-rI). All mice receiving EFP-rECs achieved normoglycemia within one
344 week, whereas only ~55% in the EFP-rI group became normoglycemic (Fig. 6B, C). An
345 intraperitoneal glucose tolerance test (IPGTT) at 5 weeks post-transplant showed that EFP-rEC
346 recipients cleared glucose almost as efficiently as healthy nondiabetic mice, whereas EFP-rI mice
347 displayed impaired glucose tolerance (Fig. 6D, E). Removing the graft-bearing EFP led to
348 recurrence of hyperglycemia in cured mice, confirming that the implanted constructs were
349 responsible for diabetes reversal. Histological analysis at 14 weeks showed well-preserved islets
350 in the EFP-rEC grafts, with a larger insulin-positive area compared to islet-alone grafts (Fig. 6F,
351 G). Immunohistochemical staining for CD31 revealed a markedly higher vessel density in EFP-

352 rEC samples compared to controls (Fig. 6F, H), suggesting enhanced vascularization and
353 engraftment.
354 Despite these encouraging results, the subsequent subcutaneous transplantation of non-
355 vascularized endocrine constructs (SQ-rEC) proved unsuccessful. None of the recipients achieved
356 normoglycemia, demonstrating that simply providing an ECM scaffold was insufficient to support
357 islet function in this poorly vascularized environment (Fig. S8). These findings confirmed that
358 prevascularization is essential for graft survival and efficacy in poorly vascularized subcutaneous
359 site.
360

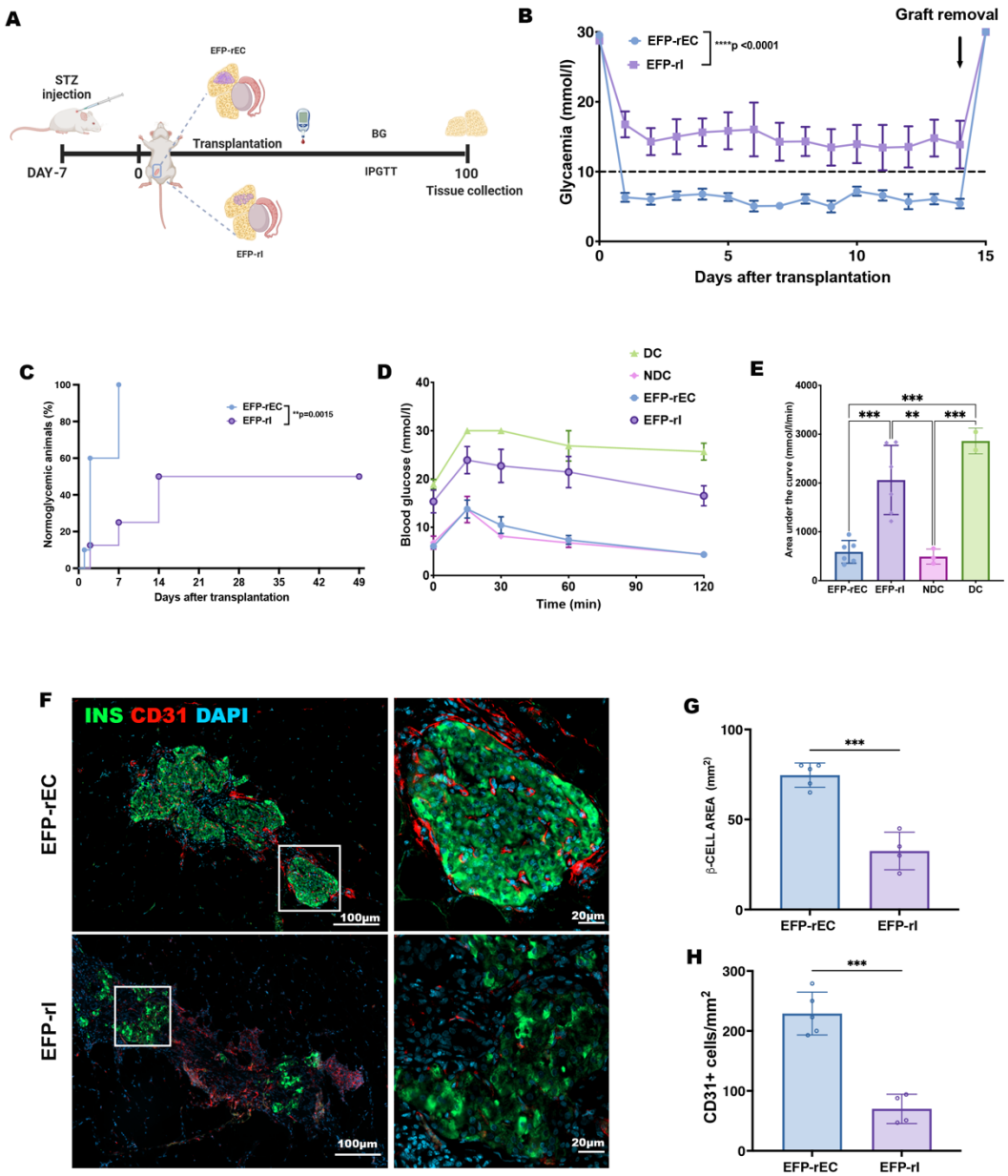

Figure 6 Function of endocrine constructs transplanted in EFP. (A) Schematic representation of the experimental setup. (B) Blood glucose measurements following transplantation. Data are presented as mean ± SEM, analyzed by two-way ANOVA with Sidak correction, ****$p < 0.0001$. (C) Kaplan-Meier analysis of the percentage of mice achieving normoglycemia (≤11 mmol/L). Differences between EFP-rEC and EFP-rI groups were assessed using a two-sided log-rank (Mantel–Cox) test, **$p = 0.0015$. (D) Blood glucose curves from the IPGTT on day 30 for EFP-

378 rEC (n = 6), EFP-rI (n = 6), non-diabetic healthy controls (NDC, n = 3), and diabetic controls (DC,
379 n = 2). Data are presented as mean ± SEM. (E) AUC analysis of IPGTT on day 30 for EFP-rEC (n
380 = 6), EFP-rI (n = 6), NDC (n = 3), and DC (n = 2). Data are presented as mean ± SD, analyzed by
381 one-way ANOVA with Tukey's correction: EFP-rEC vs. EFP-rI, ***p = 0.0006; EFP-rEC vs. DC,
382 ***p = 0.0003; EFP-rI vs. NDC, **p = 0.0021. (F) Immunohistochemical staining of retrieved
383 constructs on day 100 showing insulin (green) expression and vascularization (CD31, red). (F)
384 Representative immunofluorescent images of rat insulin (green) and mouse blood vessels (CD31,
385 red) in a retrieved constructs on day 100. (G) Percentage of insulin-positive area in EFP-rEC (n=5)
386 and EFP-rI (n=4) visualized 100 days after transplantation. Data are presented as mean ± SD, two-
387 tailed unpaired t-test, ***p=0.0002 (H) Blood vessel density in the EFP-rEC (n=5) and EFP-rI
388 (n=4); Data are presented as mean ± SD, two-tailed unpaired t-test, ***p=0.0001.
389

390 **Vascularized endocrine constructs improve glycemic control in subcutaneous transplants**

391 Building on *in vitro* findings demonstrating Amniogel's capacity to support vascular network
392 formation and enhance islet function through intercellular and cell-to-matrix communication, we
393 moved forward to evaluate the in vivo functionality of VECs in a clinically relevant but poorly
394 vascularized subcutaneous site.

395 To this end, the vascularized constructs (SQ-rVEC), were implanted subcutaneously in diabetic
396 NSG mice. For comparison, two additional groups of mice were transplanted with non-
397 vascularized constructs containing islets (SQ-rEC) or with islets alone (SQ-rI). Graft function was
398 monitored for 14 weeks (Fig. 7A). Remarkably, 96% of SQ-rVEC recipients achieved rapid
399 normoglycemia within one week, maintaining stable glucose levels significantly lower than both
400 control groups ($p<0.001$) (Fig. 7B, C). Glucose tolerance tests at day 30 showed that SQ-rVEC

group responded to the glucose challenge similarly to healthy controls and significantly better than the SQ-rEC and SQ-rI groups (Fig. 7D, E).

Graft excision led to diabetes recurrence, confirming graft function. Histological analysis revealed well-vascularized, healthy islets in SQ-rVECs, contrasting with the smaller, fragmented, and poorly vascularized islets in SQ-rECs (Figure 7G). Notably, the implanted matrix remained intact and was repopulated by host cells in both groups. Quantification of blood vessels within and surrounding the constructs (Figure 7H).

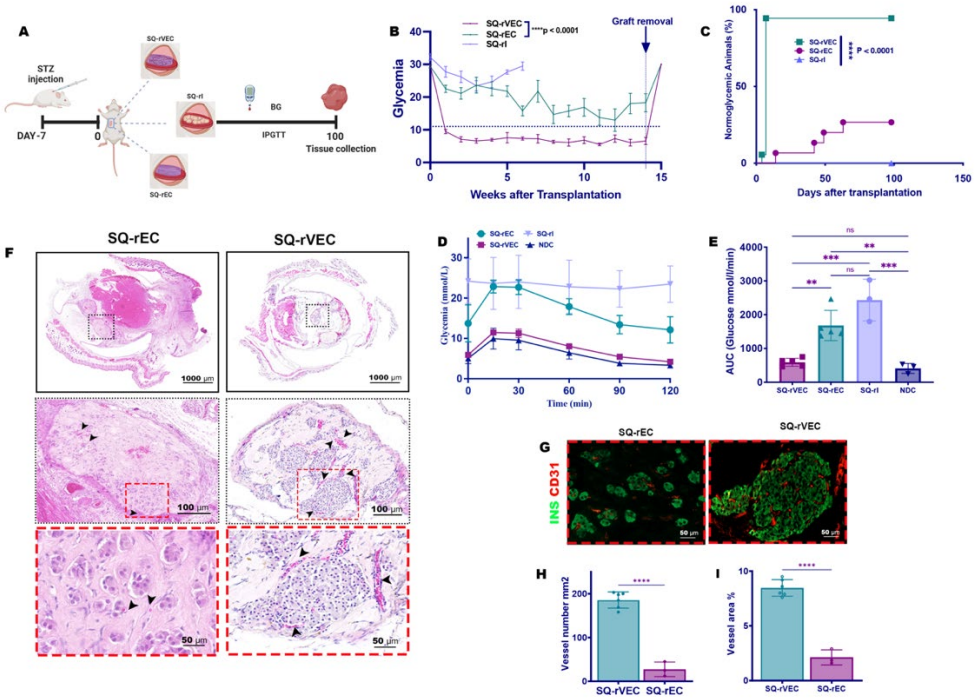

Figure 7 Performance of rat derived VECs after subcutaneous transplantation in diabetic mice. (A) Schematic representation of the experimental setup. (B) Blood glucose measurements following transplantation. Data are presented as mean ± SEM, analyzed by two-way ANOVA with Sidak correction, ****$p < 0.0001$. (C) Kaplan-Meier analysis of the percentage of mice achieving normoglycemia (≤11 mmol/L). Differences between SQ-rVEC, SQ-rEC and SQ-rI groups were

assessed using a two-sided log-rank (Mantel–Cox) test, ****p = 0.0001. (D) Graft function evaluated by IPGTT on day 30 for SQ-rVEC (n = 5), SQ-rVEC (n = 5), SQ-rI (n = 3) and NDC (n = 3). Data are presented as mean ± SEM (E) AUC analysis of IPGTT. Data are presented as mean ± SD, one-way ANOVA with Tukey's correction, SQ-rVEC v.s. SQ-rI, ***p=0.0001, SQ-rVEC vs. SQ-rEC, **p=0.0028; SQ-rVEC vs. NDC, n.s. 0.9101; SQ-rI vs. SQ-rEC, n.s. p=0.0700; SQ-rI vs. NDC, ***p=0.0001; SQ-rEC vs. NDC, **p=0.0026; (F) H&E-staining of retrieved constructs on day 100. Black arrowheads indicate blood vessels containing RBCs**;** (G) Immunohistochemical staining of retrieved constructs on day 100 showing insulin (green) expression and vascularization (CD31, red). (H, I) Blood vessel density and area percentage in the SQ-rVEC (n=6) and SQ-rEC (n=3); Data are presented as mean ± SD, two-tailed unpaired t-test, ****p<0.0001.

437 To evaluate clinical potential, we assessed subcutaneous transplantation of human islets. Given
438 mice's inherent resistance to human insulin and the requirement for a larger islet mass to achieve
439 normoglycemia in xenotransplantation studies (*38-44*), two islet-laden vascularized constructs
440 (SQ-hVEC) were implanted bilaterally into the ventral subcutaneous space. Control mice received
441 equivalent non-vascularized endocrine constructs (SQ-hEC). To minimize graft loss resulting from
442 innate immune responses known to occur even in severely immunodeficient mice (*45-47*),
443 experiments were limited to 45 days. This timeframe is clinically relevant, as islet function at one
444 month, assessed by the BETA-2 score (*48*), reliably predicts long-term transplant success (*49*).
445 SQ-hVEC group demonstrated superior outcomes, with 89% (8/9) achieving normoglycemia
446 within 14 days versus 33% (2/6) in SQ-hEC group (Fig. 8A, B). Human C-peptide levels correlated
447 with glycemic control (Fig. 8C), and glucose tolerance tests showed significantly improved
448 glucose clearance in SQ-hVEC mice (p=0.0057, Fig. 8D). All reverted to hyperglycemia upon
449 graft removal, confirming therapeutic dependence.
450 Explanted constructs showed clear differences between the two experimental groups. SQ-hVECs
451 were fully integrated with surrounding tissues and displayed well-defined, blood-perfused vascular
452 structures of various calibers surrounding the graft (Figure 8E). In contrast, SQ-hECs displayed
453 reduced vascularization and less effective integration with host tissues (Figure 8F). Histological
454 analysis showed viable islets with normal morphology in both groups (Figure 8G, H). However,
455 islets in the SQ-hVEC group were surrounded by significantly more blood vessels than those in
456 the SQ-hEC group, consistent with the observed improvements in diabetes correction (Figure 8I).
457 Immunostaining for human and mouse CD31 demonstrated the presence of chimeric blood vessels,
458 indicating anastomoses and vascular remodeling (Figure 8J). Functional maturity of the
459 vasculature was confirmed by vessels with lumens containing erythrocytes, positively stained for

460 human CD31 and α-SMA (Figure 8K). Additionally, islets in the SQ-hVEC group regained
461 laminin expression, an important extracellular matrix protein primarily deposited by endothelial
462 cells (Figure 8L). Laminin was observed both within the islets and in the surrounding tissue.
463 These findings demonstrate that prevascularizing Amniogel-based endocrine constructs
464 significantly enhances islet engraftment and function in subcutaneous transplantation sites, leading
465 to superior glycemic control.

466

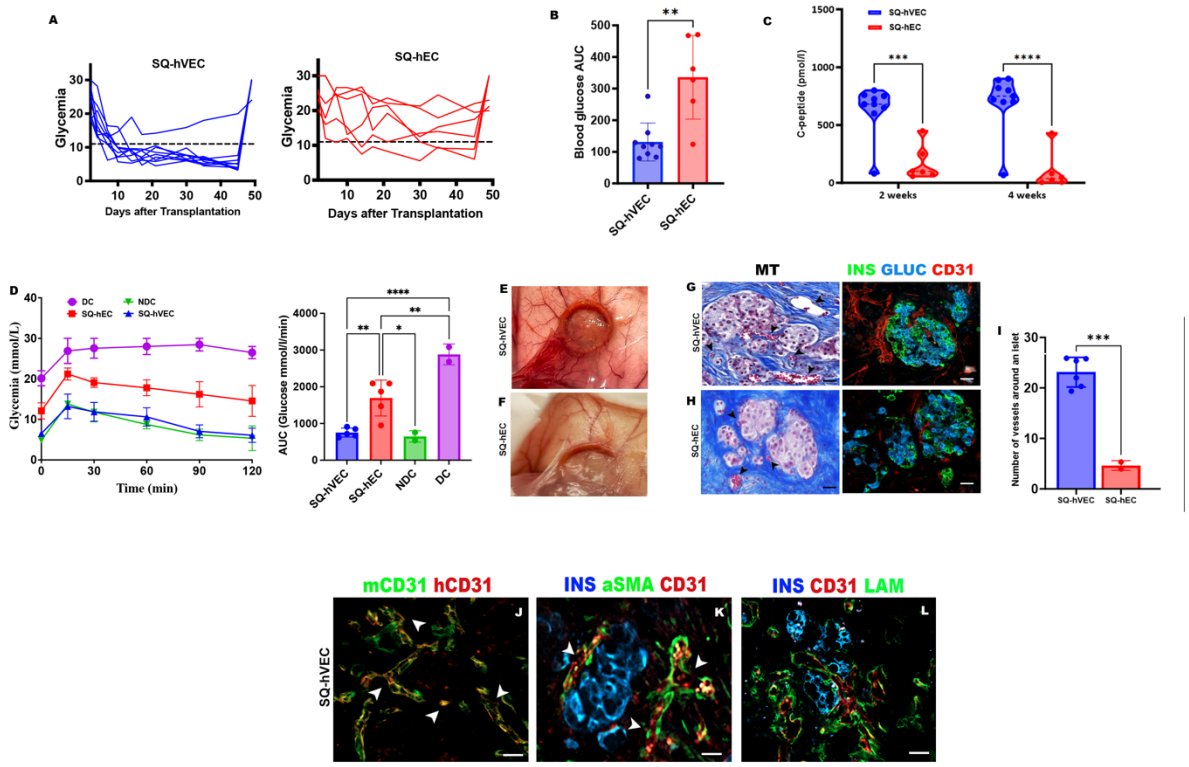

467 **Figure 8 Performance of human VECs after subcutaneous transplantation in diabetic mice**
468 (A) Blood glucose measurements following transplantation. Data are presented as mean ± SEM,
469 one-way ANOVA, SQ-hVEC vs. SQ-hEC, ****$p < 0.0001$; (B) AUC of blood glucose levels from
470 day −7 to day 30. Data are presented as mean ± SD, Unpaired t-test, p**=0.0012. (C) IPGTT

results for SQ-hVEC (n = 5), SQ-hEC (n = 5), diabetic control (DC, n = 2), and non-diabetic control (NDC, n = 2). Data are presented as mean ± SEM. (D) AUC analysis of IPGTT. Data are presented as mean ± SD, one-way ANOVA with Tukey's correction, SQ-hVEC vs. SQ-hEC., ** p =0.0057, SQ-hVEC vs. NDC, n.s., p=0.9803, SQ-rVEC vs. DC, p****<0.0001, SQ-hEC vs. NDC, p*=0.0168, SQ-hEC vs. DC, p**=0.0077 (E,F) Explanted constructs 45 days after transplant. (G, H) Cross-sectional images of retrieved constructs on day 45 showing insulin/glucagon-positive islets and vascularization of the graft. Masson's trichrome staining and fluorescence immunohistochemistry with CD31 (red) revealed blood vessels containing RBCs (black arrowheads (I) Blood vessel density in retrieved SQ-hVEC and SQ-hEC. Data are presented as mean ± SD, two-tailed unpaired t-test, ***p=0.0002. (J-L) Immunofluorescent staining of SQ-hVECs for insulin (blue), human CD31 (red), mouse CD31 (green), α-SMA (green), and laminin (green). Chimeric blood vessels and mature vessels containing RBCs are indicated by white arrowheads. Scale bars, 20 μm.

495 **DISCUSSION**

496 Recapitulating the key elements of the pancreatic niche, specificaly the ECM microenvironment
497 and vascular network is fundamental requirement for bioengineering a functional endocrine
498 pancreas (*50, 51*). While, collagen-based hydrogels and decellularized ECM matrices support
499 cellular integration and vascularization (*19, 30, 31, 52-58*), the scarcity of human ECM (*59, 60*),
500 its compromised structural integrity and cytotoxic residues associated with conventional detergent-
501 based decellularization techniques (*61, 62*) hinder clinical translation of these strategies.

502 In this study, we developed, Amniogel, a human amniotic membrane-derived hydrogel, that meets
503 these requirements. By mimicking the ECM and supporting vascularization, Amniogel recreates
504 an islet-like microenvironment. Our bioengineered endocrine constructs incorporate a collagen-
505 rich, biocompatible matrix reminiscent of the native islet niche (*63, 64*), and built-in dense, stable
506 capillary network directly interfaced with the encapsulated islets, enabling efficient glucose
507 sensing and insulin release even in the traditionally poor subcutaneous site.

508 From a translational perspective, the use of Amniogel platform offers several key advantages.
509 Amniotic membrane is an ethically sourced, established, FDA-approved clinical-grade material
510 widely used in in wound healing and ophthalmology (*65-69*). Our GMP-compliant manufacturing
511 protocol is scalable and reproducible. All reagents used in Amniogel production are available in
512 clinical-grade formulations. Additionally, its cost-effective production provides a viable
513 alternative to expensive purified ECM components. Beyond its biochemical composition,
514 Amniogel demonstrates optimal self-assembly, structural integrity supporting cell adhesion and
515 proliferation, and robust biocompatibility in immunocompetent hosts. Utilization of the host-
516 derived endothelial for vascularization is another important factor to facilitate clinical translation.
517 Taken together, these features give Amniogel a significant regulatory advantage by capitalizing
518 on existing approval frameworks rather than requiring entirely new pathways (*70*).

519 A central finding of our work is that providing an appropriate human ECM substrate significantly
520 boosts islet graft health by engaging cell–matrix survival pathways. Isolation procedures often
521 disrupt the islet ECM, triggering β-cell apoptosis via β1-integrin signaling (*71*). Previous studies
522 have demonstrated supplementing ECM proteins improves islet survival and function (*72*). In line
523 with these observations, our results showed that islets embedded in Amniogel exhibited improved
524 glucose-responsive insulin secretion and increased expression of β1-integrin, a key mediator of
525 cell-ECM adhesion critical for β-cell survival. Additionally, Amniogel-embedded islets displayed
526 reduced pro-apoptotic CASP3 and elevated anti-apoptotic BCL2 expression. These findings
527 suggest that restoring cell–matrix interactions effectively reduce β-cell apoptosis, consistent with
528 the established role of β1-integrin signaling in promoting β-cell survival (*64, 73, 74*). Furthermore,
529 we observed enhanced intercellular communication in generated VECs, via connexin-mediated
530 gap junctions. Cx-36, predominantly expressed in β-cells and facilitates coordinated insulin release
531 (*37, 75*) while, Cx-43 mediates endothelial–β-cell communication, increasing islet size and insulin
532 content (*75-77*). Our results show significant upregulation *GJD2* (5.27-fold in Amniogel; 8.08-
533 fold in vascularized constructs) and *GJA1* (6.3-fold in Amniogel; 11.4-fold in vascularized
534 constructs) compared to suspension cultures, suggesting that matrix components enhance gap-
535 junctional intercellular communication. However, it remains unclear whether this effect is
536 specifically due to laminin or broader ECM-mediated mechanisms that stabilize islets. ECM–
537 integrin interactions strongly influence connexin expression and intercellular communication in
538 other cell types (*78, 79*), suggesting a similar mechanism in our observations. Given laminin's
539 known role in integrin activation and connexin regulation (*80-82*), β1-integrin signaling may
540 promote ECM-mediated gap junction formation, thus enhancing synchronized insulin secretion in
541 β-cells. These molecular changes were associated with decreased basal insulin secretion and

542 improved glucose responsiveness in vascularized constructs, further supporting the ECM's
543 functional relevance in β-cell physiology. Additional studies are required to elucidate the precise
544 contribution of laminin–integrin signaling to gap junction assembly and to clarify whether these
545 effects arise primarily from BOEC interactions, β1-integrin signaling, or both.
546 The development of functional 3D vascular networks remains a critical hurdle in tissue engineering
547 (*83*). Amniogel promotes endothelial cell self-assembly into interconnected vascular structures,
548 creating a microenvironment conducive to sustained nutrient and oxygen delivery to encapsulated
549 islets. This spatial arrangement ensures insulin secretion occurs near blood vessels, a prerequisite
550 for optimal graft function in poorly vascularized transplant sites. Furthermore, utilization of
551 BOECs, which can be derived from the recipients themselves is a key advantage of this approach.
552 Evidence shows that humoral immune responses significantly contribute to vascularized allograft
553 failure (*84, 85*), as donor-specific antibodies (DSA) primarily target the mismatched HLA
554 molecules, expressed on graft endothelial cells (*86*). Consequently, antibody-mediated rejection
555 (AMR) predominantly affects graft microvasculature (*87*). Experimental evidence further shows
556 that endothelial chimerism—where recipient-derived vessels vascularize the graft—confers
557 resistance to AMR (*86*). Moreover, recent studies indicate allogeneic graft endothelia are also
558 susceptible to innate immune attacks by recipient natural killer (NK) cells, causing antibody-
559 independent graft injury (*88-90*). Thus, replacing donor endothelial cells with autologous BOECs
560 represents a promising strategy to reduce immune activation and prolong graft survival.
561 Importantly, BOECs from both diabetic and non-diabetic patients have been shown to enhance
562 islet engraftment with equal efficacy (*91*), reinforcing their potential for clinical use. Their
563 accessibility, robust proliferative capacity, and intrinsic ability to form functional vascular
564 networks render them highly suitable for improving engineered tissue stability and function (*92,*

565 *93*). Our findings further demonstrate that BOEC-derived vasculature surrounding islets produces
566 a basement membrane-like ECM enriched in laminin, mimicking the native islet niche. This
567 observation aligns with previous reports that β-cells rely on intra-islet endothelial cells to
568 synthesize basement membrane constituents (*94*).

569 In vivo studies confirmed that both ECM and prevascularization are essential for optimal
570 engraftment of the engineered constructs. In a marginal islet transplant model within the highly
571 vascularized epididymal fat pad, Amniogel-embedded islets exhibited significantly improved
572 engraftment compared to islets transplanted alone. However, non-vascularized constructs at the
573 same islet dose failed to restore normoglycemia, likely due to insufficient oxygenation and nutrient
574 exchange in this poorly vascularized site. These findings align with previous reports indicating
575 that although ECM integration enhances cell survival, robust vascularization remains critical for
576 effective glucose sensing and insulin secretion, particularly in the subcutaneous space, which
577 remains challenging despite clinical benefits [33, 93]. This limitation was overcome by
578 preveascularizing subcutaneously implanted endocrine constructs, resulting in significantly
579 improved islet survival and function. Notably, 96% of SQ-rVEC recipients achieved
580 normoglycemia within one week, compared to 20% in the SQ-rEC group and none in the SQ-rI
581 group. Histological analysis confirmed increased vessel density in SQ-rVEC grafts, reinforcing
582 the crucial role of vascularization for successful engraftment. Replication of these experiments
583 with human islets yielded similar results, including rapid elevation of circulating human C-peptide
584 post-transplantation. Explanted human grafts displayed excellent islet morphology, hormone
585 expression and extensive vascularization. The presence of red blood cells and α-SMA-positive
586 vessels indicated functional maturity, while chimeric vessels and restored laminin expression
587 further confirmed successful vascular integration.

588 Taken together, these results demonstrate that vascularized endocrine constructs effectively
589 address the critical limitations associated with subcutaneous islet transplantation by facilitating
590 rapid vascular integration and sustaining islet function.
591 Beyond these advantages, the versatility of Amniogel opens opportunities for broader application
592 in regenerative medicine. the versatility of Amniogel broadens its potential in regenerative
593 medicine, making it suitable for stem cell-derived insulin-producing cells, xenogeneic islets, or
594 other therapeutic cell types. Additionally, Amniogel could be modified with immunomodulatory
595 cells or molecules to optimize the local immune microenvironment and enhance engraftment
596 outcomes. Nevertheless, any modifications must be carefully optimized to maintain the established
597 safety profile of amnion-derived products and avoid introducing additional regulatory
598 complexities (*95*).
599
600 **MATERIALS AND METHODS**
601 **Study Design**
602 The objective of this study was to develop a clinically scalable, vascularized endocrine construct
603 (VEC) using a human amniotic membrane–derived hydrogel for β-cell replacement therapy.
604 Amniogel was manufactured under GMP-compatible conditions and evaluated for ECM content,
605 gelation properties, and biocompatibility. Pancreatic islets, alone or co-encapsulated with blood
606 outgrowth endothelial cells (BOECs), were embedded in Amniogel and assessed for viability,
607 vascular network formation, and insulin secretion in vitro.
608 Therapeutic efficacy was tested in streptozotocin-induced diabetic NSG mice following
609 transplantation of constructs into the epididymal fat pad or subcutaneous space. Functional
610 outcomes included glycemic control, glucose tolerance, and histological evidence of engraftment
611 and vascular integration.

612 Sample size was determined using power analysis (G*Power). Randomization was performed after
613 diabetes induction, and group allocation was concealed during transplantation. Investigators
614 assessing outcomes were blinded to group assignments when feasible, and were independent from
615 those conducting the experiments.
616
617 **Amniogel Preparation**
618 To generate Amniogel in line with GMP for future clinical use, we formulated a precise five-step
619 protocol. The process includes the harvesting of tissue, decellularization, sterilization, freeze-
620 drying, mincing, digestion, purification and neutralization (Fig. 1A).
621 Immediately after delivery, placenta was immersed in sterile PBS supplemented with antibiotics
622 (100 U/ml penicillin, 100 mg/ml streptomycin, and 0.25 mg/ml amphotericin B) and transferred
623 to the laboratory. Under sterile conditions, the human amniotic membrane (hAM) was separated,
624 rinsed to remove blood clots, and decellularized using 10X TrypLE™ Select (ThermoFisher
625 Scientific) for 40 minutes at 37°C with shaking. Decellularized membranes were washed, freeze-
626 dried, minced, and digested with 1 mg/mL porcine pepsin (Sigma Aldrich) in 0.04 N HCl for 48
627 hours at room temperature. The solubilized hAM, rreferred to as "pre-gel" was centrifuged,
628 adjusted to 10 mg/mL, aliquoted, and stored at -80°C.
629 Gelation was achieved by neutralizing pre-gels (pH 7.4) with MCDB 131 medium and $NaHCO_3$,
630 yielding 8 mg/mL Amniogel. Neutralized gel (62%) was mixed with cell suspension (38%),
631 yielding hydrogels with 5 mg/mL matrix proteins, cast into silicon molds or droplets, and
632 polymerized at 37°C for 30 minutes.
633 Amniogel batches were assessed for DNA/protein content, gel formation, and biocompatibility.
634

635 **Evaluation of Amniogel's Impact on Islet Function**

636 Rat or human islets (1000 IEQ) were suspended in 100 μL of neutralized Amniogel, loaded into
637 silicone molds, and incubated at 37 °C to facilitate gelation. The gelled constructs were cultured
638 for 7 days, with the medium replaced every other day. Suspension-cultured islets served as
639 experimental controls.

640 To evaluate the potential cytoprotective effects of Amniogel on islet cells under ischemic
641 conditions, an experiment was conducted with two groups: islet cells embedded within Amniogel
642 and control islet cells cultured without the gel. Both groups were exposed to a 16-hour hypoxic
643 environment to simulate ischemia.

644 The experiment was performed in a humidified incubator connected to a nitrogen supply,
645 maintaining a gas mixture of 1% oxygen, 5% CO_2, and 94% nitrogen. This setup accurately
646 replicated the low-oxygen environment characteristic of ischemia. The incubator temperature was
647 consistently maintained at 37 °C throughout the experiment.

648 Static glucose-stimulated insulin secretion (GSIS) assays were conducted to assess function of
649 islets. To this end, islets embedded in Amniogels or maintained in suspension culture were
650 sequentially incubated in 2.8 mM glucose (basal) and 16.7 mM glucose (stimulated) for 1 h each,
651 and supernatants were collected for insulin quantification. Human islets underwent an additional
652 stimulation step using 5 mM theophylline to enhance insulin secretion. Total insulin content was
653 extracted using acid-ethanol, and the stimulation index (SI) (stimulated/basal insulin secretion)
654 was calculated. All assays were performed in duplicate with 100 IEQ per condition.

655 **Vascular network formation in Amniogel constructs**

656 GFP-labeled BOECs (2×10^6/mL) were mixed with Amniogel, dispensed into 10–15 μL droplets,
657 and incubated at 37°C with 5% CO_2 for 30 minutes. Gelled droplets were cultured in vasculogenic

658 media (VM) composed of complete EM supplemented with 40 ng/mL VEGF-A and 20 ng/mL
659 FGF-2 for 7–14 days.

660 **Assembly of vascularized endocrine constructs**

661 To study vascular network formation and islet vascularization, isolated islets (1000 IEQ) and
662 BOECs (2×10^6) were encapsulated in 100 µL of Amniogel. The mixture was cast into silicone
663 molds to form 10 µL droplets, polymerized, and cultured at 37 °C for 7 days in optimized
664 vasculogenic medium (OVM), a 1:1 mixture of complete DMEM and VM specifically formulated
665 to maintain islet and endothelial cell viability while promoting vascular network self-assembly.
666 Controls included free islets and islet-laden Amniogels cultured under the same conditions.

667 **Live Visualization**

668 To study endothelial self-organization and network formation, live microscopy was conducted
669 using an epifluorescent microscope (DMi8 manual microscope; Leica Microsystems, Heerbrugg,
670 Switzerland). This was done without additional staining, as the endothelial cells were labeled with
671 GFP. Observations were initiated 24 hours after casting the construct, allowing sufficient time for
672 polymerization and stabilization to occur within the construct.

673 **Lumen Formation Analysis and Immunofluorescence**

674 Free-floating constructs were fixed in 4% paraformaldehyde at room temperature for 2 hours and
675 blocked with 3% FBS, 1% BSA, 0.5% Triton X-100, and 0.5% Tween for 2 hours. Primary
676 antibodies against insulin (1:50, DakoCytomation) and CD31 (1:100, DAKO) were applied
677 overnight at 4°C, followed by secondary antibodies (donkey anti-guinea pig Alexa Fluor 488 and
678 donkey anti-mouse Alexa Fluor 594, both 1:500, Jackson ImmunoResearch) for 45 minutes and
679 three PBS washes.

680 To confirm lumen formation, constructs were incubated with 0.5 mg/mL Texas red-labeled
681 Dextran (10,000 MW, ThermoFisher) in MCDB 131 medium at 37°C and 5% CO_2 overnight, fixed
682 in 4% PFA for 30 minutes, and washed with PBS.
683 Samples were cleared with RapiClear overnight at room temperature and mounted in iSpacer
684 microchambers. Fluorescent imaging was performed using a Nikon A1R confocal microscope, and
685 Z-stacks were generated with NIS-Elements Imaging Software.

686 **Implantation of Endocrine Constructs into the Epididymal Fat Pad of Diabetic Mice**

687 Immediately after isolation, 250 rat IEQs were aliquoted into 38 µl of medium, combined with 62
688 µl of neutralized Amniogel, cast into 10 µL silicone elastomer molds, and polymerized at 37°C.
689 Constructs were cultured for 24 hours. On the day of transplantation, a 0.7 cm incision was made
690 in the peritoneal wall near the genital area to expose the EFP. The islet-laden Amniogels were
691 positioned on the fat pad, folded, and reinserted into the peritoneal cavity. Each mouse received
692 four endocrine constructs containing approximately 250 IEQ (EFP-rEC; n=8). Control mice were
693 transplanted with 250 IEQ alone (EFP-rI; n=8).

694 **Subcutaneous transplantation of vascularized endocrine constructs**

695 For subcutaneous transplantation, rat or human islets (1000 IEQ) were combined with BOECs (0.2
696 $\times 10^6$) and mixed with Amniogel. For human islets, 100 µL of the mixture was cast into 9 mm
697 silicone molds; for rat islets, 10–15 µL droplets were dispensed into silicone elastomer molds. The
698 polymerized constructs were cultured at 37°C in OVM overnight.
699 Next day, mice were anesthetized with 2.5% isoflurane, and a 0.5 cm incision was made to create
700 subcutaneous pockets. A silicone ring was placed on the muscle and secured with Tisseel fibrin
701 sealant (Baxter AG) to prevent migration. Constructs were inserted into the ring, and the incision
702 was sealed with Tisseel fibrin sealant and sutured using 5–0 silk.

703 For rat islet constructs (SQ-rVEC), mice (n=18) received 8–10 microgels containing 1000 islets
704 on the left side. Controls included non-vascularized endocrine constructs (SQ-rEC) with identical
705 islet quantities (n=15) and subcutaneously implanted naked islets (n=6).
706 For human islet constructs (SQ-hVEC; n=9), a single construct. (9mm diameter) containing 1000
707 IEQ was implanted on each side (2000 IEQ total). Mice transplanted with nonvascularized
708 constructs (SQ-hEC; n=6), containing equal number of islets served as controls.

709 **Histopathological analysis and immunostaining**

710 Explanted grafts were fixed in 4% paraformaldehyde and either paraffin-embedded or snap-frozen
711 in OCT compound (Tissue-Tek, Sakura Finetek). Serial 5 µm sections (10 per graft) were prepared
712 for hematoxylin-eosin (H&E), Mason Trichrome (MT), or immunofluorescence staining.
713 For immunostaining, sections were permeabilized, blocked, and incubated overnight with primary
714 antibodies against insulin (1:50, DakoCytomation), glucagon (1:4000, Sigma-Aldrich), human-
715 specific CD31 (1:50, DakoCytomation), CD31 (1:50, Abcam), CD34 (1:2000, Abcam), laminin
716 (1:30, Sigma-Aldrich), collagen IV (1:30, Bio-Rad), CD45 (1:100, Abcam), and CD11b (1:200,
717 Abcam). Secondary antibodies included goat anti-mouse, anti-rabbit, anti-guinea pig (1:300,
718 ThermoFisher Scientific), goat anti-guinea pig (1:500, Jackson ImmunoResearch), donkey anti-
719 rabbit Alexa Fluor 594 (1:500, Jackson ImmunoResearch), and rat anti-mouse Alexa Fluor 594
720 (1:200, Abcam). Sections were mounted with DAPI-containing mounting medium (ProTaqs
721 MountFluor Anti-Fading).
722 Images were captured using a Zeiss Axioscan.Z1 slide scanner, and morphometric and
723 fluorescence analyses were performed with ImageJ software.
724 In H&E and MT-stained images, blood vessels were identified by luminal structures containing
725 erythrocytes. Vessel numbers within grafts were quantified, and vessel/graft and vessel/β-cell

726 ratios were calculated as percentages of graft and insulin-positive areas. Human vasculature was
727 confirmed by erythrocyte-containing vessels positive for human CD31 and α-SMA staining.
728

729 **Statistical analysis**

730 Statistical analyses were performed using GraphPad Prism 10.0. All experiments were repeated at
731 least three times. Specific statistical tests are detailed in the figure legends, with significance
732 defined as $P < 0.05$.

733 **List of Supplementary Materials**

734 Materials and Methods
735 Fig. S1 or Fig S9
736 Table S1
737 References (*1,2*)
738
739
740
741
742
743
744
745
746
747
748

749 **References and Notes**

750

751 1. L. A. DiMeglio, C. Evans-Molina, R. A. Oram, Type 1 diabetes. *Lancet* **391**, 2449-2462 (2018).
752 2. F. B. Barton *et al.*, Improvement in outcomes of clinical islet transplantation: 1999-2010.
753 *Diabetes care* **35**, 1436-1445 (2012).
754 3. A. M. Shapiro, M. Pokrywczynska, C. Ricordi, Clinical pancreatic islet transplantation. *Nature*
755 *reviews. Endocrinology* **13**, 268-277 (2017).
756 4. B. W. Paty, J. S. Harmon, C. L. Marsh, R. P. Robertson, Inhibitory effects of immunosuppressive
757 drugs on insulin secretion from HIT-T15 cells and Wistar rat islets. *Transplantation* **73**, 353-357
758 (2002).
759 5. L. Reid, F. Baxter, S. Forbes, Effects of islet transplantation on microvascular and macrovascular
760 complications in type 1 diabetes. *Diabetic medicine : a journal of the British Diabetic Association*
761 **38**, e14570 (2021).
762 6. E. A. Ryan, B. W. Paty, P. A. Senior, A. M. Shapiro, Risks and side effects of islet transplantation.
763 *Curr Diab Rep* **4**, 304-309 (2004).
764 7. M. Biarnés, M. Montolio, V. Nacher, M. Raurell, J. Soler, E. Montanya, Beta-cell death and mass
765 in syngeneically transplanted islets exposed to short- and long-term hyperglycemia. *Diabetes* **51**,
766 66-72 (2002).
767 8. G. L. Jones, M. T. Juszczak, S. J. Hughes, P. Kooner, S. H. Powis, M. Press, Time course and
768 quantification of pancreatic islet revascularization following intraportal transplantation. *Cell*
769 *transplantation* **16**, 505-516 (2007).
770 9. W. Moritz *et al.*, Apoptosis in hypoxic human pancreatic islets correlates with HIF-1alpha
771 expression. *Faseb j* **16**, 745-747 (2002).
772 10. J. Tjernberg, K. N. Ekdahl, J. D. Lambris, O. Korsgren, B. Nilsson, Acute antibody-mediated
773 complement activation mediates lysis of pancreatic islets cells and may cause tissue loss in
774 clinical islet transplantation. *Transplantation* **85**, 1193-1199 (2008).
775 11. D. M. Berman *et al.*, Bioengineering the Endocrine Pancreas: Intraomental Islet Transplantation
776 Within a Biologic Resorbable Scaffold. *Diabetes* **65**, 1350-1361 (2016).
777 12. E. Cantarelli *et al.*, Bone marrow as an alternative site for islet transplantation. *Blood* **114**, 4566-
778 4574 (2009).
779 13. Z. Kakabadze, S. Gupta, D. Brandhorst, O. Korsgren, E. Berishvili, Long-term engraftment and
780 function of transplanted pancreatic islets in vascularized segments of small intestine. *Transpl Int*
781 **24**, 175-183 (2011).
782 14. Z. Kakabadze *et al.*, Correction of diabetes mellitus by transplanting minimal mass of syngeneic
783 islets into vascularized small intestinal segment. *Am J Transplant* **13**, 2550-2557 (2013).
784 15. Z. Kakabadze, K. Shanava, C. Ricordi, A. M. Shapiro, S. Gupta, E. Berishvili, An isolated venous sac
785 as a novel site for cell therapy in diabetes mellitus. *Transplantation* **94**, 319-324 (2012).
786 16. F. Pattou, J. Kerr-Conte, D. Wild, GLP-1-receptor scanning for imaging of human beta cells
787 transplanted in muscle. *The New England journal of medicine* **363**, 1289-1290 (2010).
788 17. E. Rafael *et al.*, Intramuscular autotransplantation of pancreatic islets in a 7-year-old child: a 2-
789 year follow-up. *Am J Transplant* **8**, 458-462 (2008).
790 18. A. Sterkers *et al.*, Islet survival and function following intramuscular autotransplantation in the
791 minipig. *Am J Transplant* **13**, 891-898 (2013).
792 19. M. Yu *et al.*, Islet transplantation in the subcutaneous space achieves long-term euglycaemia in
793 preclinical models of type 1 diabetes. *Nature metabolism* **2**, 1013-1020 (2020).
794 20. M. J. Quizon, A. J. García, Engineering β Cell Replacement Therapies for Type 1 Diabetes:
795 Biomaterial Advances and Considerations for Macroscale Constructs. *Annual review of*
796 *pathology* **17**, 485-513 (2022).
797 21. R. Hanna, E. Berishvili, Advances and challenges of endocrine pancreas bioengineering. *Current*
798 *Opinion in Endocrine and Metabolic Research* **23**, 100320 (2022).

22. T. Berney *et al.*, From islet of Langerhans transplantation to the bioartificial pancreas. *Presse medicale (Paris, France : 1983)*, 104139 (2022).
23. A. D. Agulnick *et al.*, Insulin-Producing Endocrine Cells Differentiated In Vitro From Human Embryonic Stem Cells Function in Macroencapsulation Devices In Vivo. *Stem cells translational medicine* **4**, 1214-1222 (2015).
24. P. O. Carlsson *et al.*, Transplantation of macroencapsulated human islets within the bioartificial pancreas βAir to patients with type 1 diabetes mellitus. *Am J Transplant* **18**, 1735-1744 (2018).
25. A. M. J. Shapiro *et al.*, Insulin expression and C-peptide in type 1 diabetes subjects implanted with stem cell-derived pancreatic endoderm cells in an encapsulation device. *Cell reports. Medicine* **2**, 100466 (2021).
26. M. Barillaro, M. Schuurman, R. Wang, β1-Integrin—A Key Player in Controlling Pancreatic Beta-Cell Insulin Secretion via Interplay With SNARE Proteins. *Endocrinology* **164**, (2022).
27. L. Rosenberg, R. Wang, S. Paraskevas, D. Maysinger, Structural and functional changes resulting from islet isolation lead to islet cell death. *Surgery* **126**, 393-398 (1999).
28. M. Riopel, R. Wang, Collagen matrix support of pancreatic islet survival and function. *Frontiers in bioscience (Landmark edition)* **19**, 77-90 (2014).
29. S. Saleem, J. Li, S. P. Yee, G. F. Fellows, C. G. Goodyer, R. Wang, beta1 integrin/FAK/ERK signalling pathway is essential for human fetal islet cell differentiation and survival. *The Journal of pathology* **219**, 182-192 (2009).
30. C. H. Stephens *et al.*, Oligomeric collagen as an encapsulation material for islet/β-cell replacement: effect of islet source, dose, implant site, and administration format. *Am J Physiol Endocrinol Metab* **319**, E388-e400 (2020).
31. A. E. Vlahos, N. Cober, M. V. Sefton, Modular tissue engineering for the vascularization of subcutaneously transplanted pancreatic islets. *Proceedings of the National Academy of Sciences of the United States of America* **114**, 9337-9342 (2017).
32. D. M. Tremmel *et al.*, A human pancreatic ECM hydrogel optimized for 3-D modeling of the islet microenvironment. *Scientific Reports* **12**, 7188 (2022).
33. D. A. Baidal *et al.*, Bioengineering of an Intraabdominal Endocrine Pancreas. *The New England journal of medicine* **376**, 1887-1889 (2017).
34. F. Lebreton *et al.*, Insulin-producing organoids engineered from islet and amniotic epithelial cells to treat diabetes. *Nature communications* **10**, 4491 (2019).
35. P. M. Crapo, T. W. Gilbert, S. F. Badylak, An overview of tissue and whole organ decellularization processes. *Biomaterials* **32**, 3233-3243 (2011).
36. A. Citro *et al.*, Biofabrication of a vascularized islet organ for type 1 diabetes. *Biomaterials* **199**, 40-51 (2019).
37. W. R. Loewenstein, Junctional intercellular communication: the cell-to-cell membrane channel. *Physiol Rev* **61**, 829-913 (1981).
38. J. Chen, J. E. Gunton, Beta-cell function and human islet transplantation: can we improve? *J Endocrinol* **248**, R99-r112 (2021).
39. P. Dunér *et al.*, Adhesion G Protein-Coupled Receptor G1 (ADGRG1/GPR56) and Pancreatic β-Cell Function. *J Clin Endocrinol Metab* **101**, 4637-4645 (2016).
40. O. Cabrera, D. M. Berman, N. S. Kenyon, C. Ricordi, P. O. Berggren, A. Caicedo, The unique cytoarchitecture of human pancreatic islets has implications for islet cell function. *Proceedings of the National Academy of Sciences of the United States of America* **103**, 2334-2339 (2006).
41. P. Rorsman, F. M. Ashcroft, Pancreatic β-Cell Electrical Activity and Insulin Secretion: Of Mice and Men. *Physiol Rev* **98**, 117-214 (2018).

845 42. M. Brissova *et al.*, Human Islets Have Fewer Blood Vessels than Mouse Islets and the Density of
846 Islet Vascular Structures Is Increased in Type 2 Diabetes. *J Histochem Cytochem* **63**, 637-645
847 (2015).
848 43. C. Dai *et al.*, Islet-enriched gene expression and glucose-induced insulin secretion in human and
849 mouse islets. *Diabetologia* **55**, 707-718 (2012).
850 44. A. R. Pepper, C. Gall, D. M. Mazzuca, C. W. Melling, D. J. White, Diabetic rats and mice are
851 resistant to porcine and human insulin: flawed experimental models for testing islet xenografts.
852 *Xenotransplantation* **16**, 502-510 (2009).
853 45. M. Wunderlich *et al.*, A xenograft model of macrophage activation syndrome amenable to anti-
854 CD33 and anti-IL-6R treatment. *JCI Insight* **1**, e88181 (2016).
855 46. M. Hu, W. J. Hawthorne, S. Yi, P. J. O'Connell, Cellular Immune Responses in Islet Xenograft
856 Rejection. *Front Immunol* **13**, 893985 (2022).
857 47. M. Vadori, E. Cozzi, Immunological challenges and therapies in xenotransplantation. *Cold Spring*
858 *Harb Perspect Med* **4**, a015578 (2014).
859 48. A. Lam *et al.*, Estimation of Early Graft Function Using the BETA-2 Score Following Clinical Islet
860 Transplantation. *Transpl Int* **35**, 10335 (2022).
861 49. M. Chetboun *et al.*, Association between primary graft function and 5-year outcomes of islet
862 allogeneic transplantation in type 1 diabetes: a retrospective, multicentre, observational cohort
863 study in 1210 patients from the Collaborative Islet Transplant Registry. *Lancet Diabetes*
864 *Endocrinol* **11**, 391-401 (2023).
865 50. S. E. Townsend, M. Gannon, Extracellular Matrix–Associated Factors Play Critical Roles in
866 Regulating Pancreatic β-Cell Proliferation and Survival. *Endocrinology* **160**, 1885-1894 (2019).
867 51. C. Pignatelli, F. Campo, A. Neroni, L. Piemonti, A. Citro, Bioengineering the Vascularized
868 Endocrine Pancreas: A Fine-Tuned Interplay Between Vascularization, Extracellular-Matrix-Based
869 Scaffold Architecture, and Insulin-Producing Cells. *Transpl Int* **35**, 10555 (2022).
870 52. A. Citro *et al.*, Directed self-assembly of a xenogeneic vascularized endocrine pancreas for type 1
871 diabetes. *Nature communications* **14**, 878 (2023).
872 53. J. D. Weaver *et al.*, Vasculogenic hydrogel enhances islet survival, engraftment, and function in
873 leading extrahepatic sites. *Sci Adv* **3**, e1700184 (2017).
874 54. E. A. Phelps, K. L. Templeman, P. M. Thulé, A. J. García, Engineered VEGF-releasing PEG-MAL
875 hydrogel for pancreatic islet vascularization. *Drug Deliv Transl Res* **5**, 125-136 (2015).
876 55. D. M. Tremmel *et al.*, A human pancreatic ECM hydrogel optimized for 3-D modeling of the islet
877 microenvironment. *Sci Rep* **12**, 7188 (2022).
878 56. X. Hu, Z. Wu, Z. Zhang, H. Yao, D.-A. Wang, Type II collagen scaffolds for tissue engineering.
879 *Communications Materials* **5**, 149 (2024).
880 57. S. Ullah, I. Zainol, Fabrication and applications of biofunctional collagen biomaterials in tissue
881 engineering. *Int J Biol Macromol* **298**, 139952 (2025).
882 58. M. Abedi, M. Shafiee, F. Afshari, H. Mohammadi, Y. Ghasemi, Collagen-Based Medical Devices
883 for Regenerative Medicine and Tissue Engineering. *Appl Biochem Biotechnol* **196**, 5563-5603
884 (2024).
885 59. R. Tamburrini *et al.*, Detergent-Free Decellularization of the Human Pancreas for Soluble
886 Extracellular Matrix (ECM) Production. *J Vis Exp*, (2020).
887 60. L. Somasekhar, L. G. Griffiths, Current Challenges and Future Promise for Use of Extracellular
888 Matrix Scaffold to Achieve the Whole Organ Tissue Engineering Moonshot. *Stem cells*
889 *translational medicine* **12**, 588-602 (2023).
890 61. J. Fernández-Pérez, M. Ahearne, The impact of decellularization methods on extracellular matrix
891 derived hydrogels. *Scientific Reports* **9**, 14933 (2019).

892 62. M. Kasravi *et al.*, Immunogenicity of decellularized extracellular matrix scaffolds: a bottleneck in
893 tissue engineering and regenerative medicine. *Biomater Res* **27**, 10 (2023).
894 63. A. Asthana *et al.*, Comprehensive characterization of the human pancreatic proteome for
895 bioengineering applications. *Biomaterials* **270**, 120613 (2021).
896 64. Z. Li *et al.*, Proteome-wide and matrisome-specific alterations during human pancreas
897 development and maturation. *Nature communications* **12**, 1020 (2021).
898 65. Z. Hu *et al.*, Biological importance of human amniotic membrane in tissue engineering and
899 regenerative medicine. *Mater Today Bio* **22**, 100790 (2023).
900 66. F. Dadkhah Tehrani, A. Firouzeh, I. Shabani, A. Shabani, A Review on Modifications of Amniotic
901 Membrane for Biomedical Applications. *Frontiers in bioengineering and biotechnology* **8**, 606982
902 (2020).
903 67. M. Doucette *et al.*, Early Advanced Therapy for Diabetic Foot Ulcers in High Amputation Risk
904 Veterans: A Cohort Study. *Int J Low Extrem Wounds* **21**, 111-119 (2022).
905 68. I. Schmiedova, Z. Ozanova, E. Stastna, L. Kiselakova, B. Lipovy, S. Forostyak, Case Report: Freeze-
906 Dried Human Amniotic Membrane Allograft for the Treatment of Chronic Wounds: Results of a
907 Multicentre Observational Study. *Frontiers in bioengineering and biotechnology* **9**, 649446
908 (2021).
909 69. B. Lipový, M. Hladík, P. Štourač, S. Forostyak, Case Report: Wound Closure Acceleration in a
910 Patient With Toxic Epidermal Necrolysis Using a Lyophilised Amniotic Membrane. *Frontiers in*
911 *bioengineering and biotechnology* **9**, 649317 (2021).
912 70. E. Berishvili *et al.*, ESOT Roadmap for Advanced Therapy Medicinal Products in Transplantation:
913 Navigating Regulatory Challenges to Enhance Access and Care. *Transpl Int* **37**, 13485 (2024).
914 71. S. E. Cross *et al.*, Key Matrix Proteins Within the Pancreatic Islet Basement Membrane Are
915 Differentially Digested During Human Islet Isolation. *Am J Transplant* **17**, 451-461 (2017).
916 72. L. A. Llacua, M. M. Faas, P. de Vos, Extracellular matrix molecules and their potential
917 contribution to the function of transplanted pancreatic islets. *Diabetologia* **61**, 1261-1272
918 (2018).
919 73. M. M. Riopel, J. Li, S. Liu, A. Leask, R. Wang, β1 integrin–extracellular matrix interactions are
920 essential for maintaining exocrine pancreas architecture and function. *Laboratory Investigation*
921 **93**, 31-40 (2013).
922 74. J. Peart, J. Li, H. Lee, M. Riopel, Z. C. Feng, R. Wang, Critical role of β1 integrin in postnatal beta-
923 cell function and expansion. *Oncotarget* **8**, 62939-62952 (2017).
924 75. C. P. Carvalho *et al.*, Beta cell coupling and connexin expression change during the functional
925 maturation of rat pancreatic islets. *Diabetologia* **53**, 1428-1437 (2010).
926 76. P. Klee *et al.*, Connexin implication in the control of the murine beta-cell mass. *Pediatr Res* **70**,
927 142-147 (2011).
928 77. N. L. Farnsworth, R. K. Benninger, New insights into the role of connexins in pancreatic islet
929 function and diabetes. *FEBS Lett* **588**, 1278-1287 (2014).
930 78. Y. Guo, C. Martinez-Williams, C. E. Yellowley, H. J. Donahue, D. E. Rannels, Connexin expression
931 by alveolar epithelial cells is regulated by extracellular matrix. *Am J Physiol Lung Cell Mol Physiol*
932 **280**, L191-202 (2001).
933 79. S. Imbeault *et al.*, The extracellular matrix controls gap junction protein expression and function
934 in postnatal hippocampal neural progenitor cells. *BMC Neurosci* **10**, 13 (2009).
935 80. H. Peiris, C. S. Bonder, P. T. Coates, D. J. Keating, C. F. Jessup, The β-cell/EC axis: how do islet
936 cells talk to each other? *Diabetes* **63**, 3-11 (2014).
937 81. G. Burganova, C. Bridges, P. Thorn, L. Landsman, The Role of Vascular Cells in Pancreatic Beta-
938 Cell Function. *Frontiers in endocrinology* **12**, 667170 (2021).

82. G. Parnaud, E. Hammar, D. G. Rouiller, M. Armanet, P. A. Halban, D. Bosco, Blockade of beta1 integrin-laminin-5 interaction affects spreading and insulin secretion of rat beta-cells attached on extracellular matrix. *Diabetes* **55**, 1413-1420 (2006).
83. L. M. Fonseca, N. Krause, F. Lebreton, E. Berishvili, Recreating the Endocrine Niche: Advances in Bioengineering the Pancreas. *Artif Organs*, (2025).
84. J. Sellarés *et al.*, Understanding the causes of kidney transplant failure: the dominant role of antibody-mediated rejection and nonadherence. *Am J Transplant* **12**, 388-399 (2012).
85. E. Pouliquen *et al.*, Recent advances in renal transplantation: antibody-mediated rejection takes center stage. *F1000Prime Rep* **7**, 51 (2015).
86. C. C. Chen *et al.*, Endothelial chimerism and vascular sequestration protect pancreatic islet grafts from antibody-mediated rejection. *J Clin Invest* **128**, 219-232 (2018).
87. M. Naesens *et al.*, The Banff 2022 Kidney Meeting Report: Reappraisal of microvascular inflammation and the role of biopsy-based transcript diagnostics. *Am J Transplant* **24**, 338-349 (2024).
88. X. Charmetant, G. J. Pettigrew, O. Thaunat, Allorecognition Unveiled: Integrating Recent Breakthroughs Into the Current Paradigm. *Transpl Int* **37**, 13523 (2024).
89. A. Koenig *et al.*, Missing self triggers NK cell-mediated chronic vascular rejection of solid organ transplants. *Nature communications* **10**, 5350 (2019).
90. O. Thaunat, Natural killer cell-mediated innate microvascular rejection. *Nat Rev Nephrol* **20**, 489-490 (2024).
91. V. Coppens *et al.*, Human blood outgrowth endothelial cells improve islet survival and function when co-transplanted in a mouse model of diabetes. *Diabetologia* **56**, 382-390 (2013).
92. T. Mathur *et al.*, Organ-on-chips made of blood: endothelial progenitor cells from blood reconstitute vascular thromboinflammation in vessel-chips. *Lab Chip* **19**, 2500-2511 (2019).
93. C. Olgasi *et al.*, Efficient and safe correction of hemophilia A by lentiviral vector-transduced BOECs in an implantable device. *Mol Ther Methods Clin Dev* **23**, 551-566 (2021).
94. H. Peiris, C. S. Bonder, P. T. H. Coates, D. J. Keating, C. F. Jessup, The β-Cell/EC Axis: How Do Islet Cells Talk to Each Other? *Diabetes* **63**, 3-11 (2013).
95. R. L. Thom, A. J. Cronin, Legal and Regulatory Challenges for Emerging Regenerative Medicine Solutions for Diabetes. *Transplantation* **108**, 1072-1079 (2024).

Funding: This work is supported by grants from the European Commission (Horizon 2020 Framework Program; VANGUARD grant 874700), the Breakthrough T1D, formerly JDRF (JDRF; grant 3-SRA-2020-926-S-B and 3-SRA-2023-1441-S-B) and the Swiss National Science Foundation (grant 310030_213013 and CRSII5_209417).

Author contributions: E.B. conceptualized and supervised the project.; E.B. and K.B. developed the methodology; K.B., F.L. and M.H. performed animal breeding and conducted experiments;

K.B., F.L., M.H., R.H., J.B., A.M., L.M.F., and F.C. performed analysis of results; K.B., and M.H. performed visualization.; A.F. and A.C. produced BOECs; E.B. K.B. and F.L. wrote the original draft.; A.F., L.P., O.T., J.S, M.C. and E.B. contributed to the design of the experiments.; A.F., C.O., J.B., A.M., L.M.F., M.C., B.MT., L.P., A.C., O.T., J.S., M.H., L.WB., P.C. and VANGUARD consortium critically reviewed and edited the paper.

Competing interests: Authors declare that they have no competing interests.

Data and materials availability: All data are available in the main text or the supplementary materials.

§ Members of the VANGUARD consortium are as follows:

Thierry Berney, Nicerine Krause, Shota Tsikhiseli, University of Geneva, Department of Surgery, Geneva, Switzerland

Alessia Cucci, Chiara Borsotti, Simone Assanelli, Department of Health Sciences, University of Piemonte Orientale, Novara, Italy

Cataldo Pignatelli, IRCCS Ospedale San Raffaele, Diabetes Research Institute, Milano, Italy

Emma Massey, Dide de Jongh, Erasmus MC, University Medical Centre Rotterdam, The Netherlands

Eline Bunnik, Dept. of Medical Ethics, Philosophy and History of Medicine, University Medical Centre Rotterdam, The Netherlands

Antonia J. Cronin, King's College, London, UK

Devi Mey, Chiara Parisotto European Society for Organ Transplantation, Padova, Italy

Patrick Kugelmeier, Petra Wolint, Kugelmeiers AG, Erlenbach, Switzerland

Margaryta Schaltegger, Julia Götz, Jeanette Müller, Accelopment Switzerland Ltd.